RAPID COMMUNICATIONS

PHYSICAL REVIEW E VOLUME 51, NUMBER 4 APRIL 1995

Polarized angular distributions of parametric x radiation and vacuum-ultraviolet transition radiation from relativistic electrons

R. B. Fiorito,[1,*] D. W. Rule,[1] M. A. Piestrup,[2] X. K. Maruyama,[3] R. M. Silzer,[4] D. M. Skopik,[4] and A. V. Shchagin[5]

[1]*Naval Surface Warfare Center, Carderock Division, 10901 New Hampshire Avenue, Silver Spring, Maryland 20903-5640*

[2]*Adelphi Technology Inc., 2181 Park Boulevard, Palo Alto, California 94301*

[3]*Naval Postgraduate School, Monterey, California 93943*

[4]*Saskatchewan Accelerator Laboratory, Saskatoon, Saskatchewan, Canada S7N OWO*

[5]*Kharkov Institute of Physical Science and Technology, 310108 Ukraine*

(Received 5 August 1994; revised manuscript received 4 January 1995)

We present quantifiable images of the angular distributions (AD's) of parametric x radiation (PXR), and vacuum-ultraviolet transition radiation (vuv TR) from 230 MeV electrons interacting with a silicon crystal. Both AD's are highly polarized. The vuv TR and optical TR data provide measurements of the beam energy and effective divergence angle. Using these quantities and separately known values of the electronic susceptibility $|\chi_0|$, we show that the measured PXR AD is in good agreement with the predictions of single crystal theory. Our analysis suggests a method to measure $|\chi_0|$ using PXR AD's.

PACS number(s): 41.60.−m, 78.70.Ck

The production of x rays via the interaction of charged particles with crystals, known as parametric x radiation [1,2] (PXR), can be described as the diffraction of virtual photons of the electromagnetic field of a charged particle by the crystal planes. The unique properties of PXR—tunability, quasimonochromaticity, and, for relativistic particles, high spectral brightness per electron [3,4]—make it a potentially useful source of x rays for a wide variety of applications.

Predictions [1,2] of the spectral and angular features of the radiation have been generally verified for single crystals [5–13]. However, some large quantitative discrepancies between theory and experiment have been shown with regard to the effects of multiple scattering (MS) [12,13] and mosaicity [13].

Measurements of the angular distribution (AD) of PXR, which is highly sensitive both to the properties of the beam (energy, divergence, MS) and the crystal's electric susceptibility $|\chi_0|$, can provide a stringent test of the theory. However, relatively few quantitative studies [5–8] of the AD have been made because of the difficulty in making the measurements. These are usually done at a fixed Bragg angle θ_B, by scanning an aperture across the AD, and acquiring a spectrum at each aperture position. The available data show varying degrees of success in comparison to theory.

The desire for AD data, which is more easily obtained and sufficiently quantitative to test the theory, has led to attempts to image the complete PXR AD. However, previous efforts have not been entirely successful [10,14]. Furthermore, in order to input the beam divergence and multiple scattering angle into the theory, it is desirable to independently determine these properties, which have not all been known for the experiments reported so far.

Transition radiation (TR) [15], which is produced by charged particles crossing a boundary between media with different dielectric constants, is a related, but better understood phenomenon than PXR. TR is broadband (microwave to x ray), and like PXR, for relativistic particles, has a narrowly directed AD. In contrast to PXR, however, the angle of peak emission and the width of the AD of TR are solely determined by the properties of the beam. TR from relativistic beams has been studied extensively both in the x-ray [15–17] (XTR) and optical [18,19] (OTR) regions of the spectra. XTR has been shown to be a useful high energy particle discriminator [20], and radiation source [21]; OTR, a precise beam energy [18], profile [18] and emittance [19] diagnostic. Previous studies [15] of TR in the vuv have been performed only at nonrelativistic electron beam energies ($\lesssim$100 keV).

We report here clear, quantifiable images of the AD pattern of PXR and vuv TR from relativistic particles. PXR is observed at 90° from the (022) planes of a thin (20 μm) silicon crystal in a Laue geometry. vuv TR and OTR are observed from the surface of the crystal. The experiments are performed at the Saskatchewan Accelerator Laboratory (SAL) with a 230 MeV, 15 μA electron beam. The PXR and vuv TR AD's are separately imaged with a cesium iodide coated (5 μm) microchannel plate detector (CsI MCP) under identical beam conditions. An analysis of the vuv TR AD provides an independent measure of the beam's energy E_b and the effective divergence σ_{eff} due to the finite size of the beam. The beam size is determined from a measurement of the beam's spatial distribution using OTR. Knowledge of these beam properties is used to isolate the effect of susceptibility on the PXR AD.

A schematic of the experimental setup is shown in Fig. 1. The surface of the Si is parallel to the (100) planes, which are perpendicular to the (022) planes. $\theta_B=45°$ with respect to the latter, so that the PXR emerges on the far side (Laue condition) of the crystal at 90° with respect to the beam's velocity vector $\mathbf{v}_b$. The crystal is mounted on a remotely controlled goniometer. A He-Ne laser and a pinhole are used to position the electron beam and orient the crystal planes with respect to $\mathbf{v}_b$. The overall error in positioning the planes is <1.0 mrad. The OTR produced by the beam from the polished surface of the crystal facing the beam is so intense that it can be imaged with a standard lens and vidicon camera, and is observable within several degrees of the specular reflection angle (45°).

*Electronic address: fiorito@oasys.dt.navy.mil

 © 1995 The American Physical Society

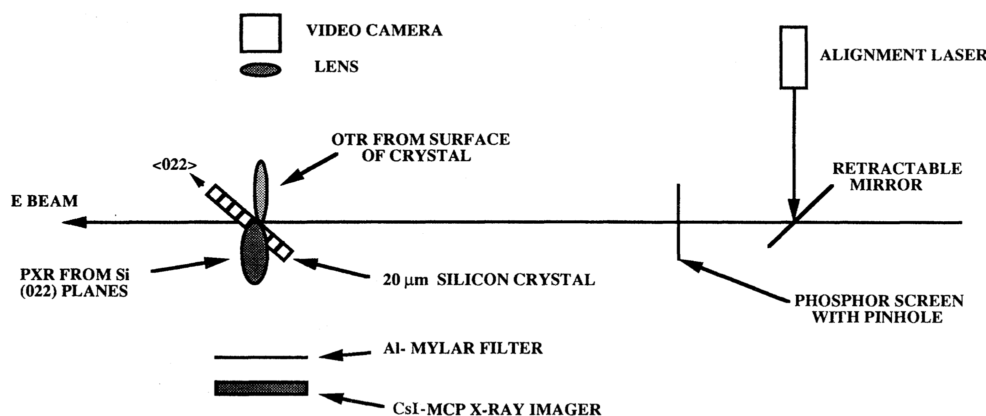

FIG. 1. Schematic diagram of the experimental setup to observe PXR from (022) planes of silicon.

The CsI MCP imaging detector, manufactured by X-ray Specialty Instruments Inc. (XSI), Ann Arbor, MI, is 42 mm in diameter, and is located in vacuum at 90° to the beam line, 564 mm from the crystal. A 7-μm aluminized Mylar filter, which is used to block any optical or uv radiation from the crystal, can be remotely inserted in front of the detector. The detector converts the input x-ray or vuv AD pattern to a visible light image on a phospor coating on the rear side of the MCP, which is then focused onto a charge coupled device (CCD) video camera. A maximum of 128 video frames can be digitized and added dynamically by an integrator. These are then transferred to the disk of a computer for further processing.

Figure 2(a) shows an image of the AD of the PXR colored coded with black as the lowest intensity value (0) and purple the highest (256). The peak number of counts, $N_{\text{peak}} \sim 30$ is scaled to 256. The image is obtained by adding 1280 frames (10×128 integrations) and subtracting an equal number of background frames. The background, which is dominated by electronic noise in the CCD, is obtained by rotating the crystal so that the PXR pattern is directed off the detector. The pattern is nearly 100% polarized in the vertical (θ_y) direction, i.e., perpendicular to the plane formed by $\mathbf{v}_b$ and the (022) direction. This result is predicted from PXR theory [1,2] when $\theta_B = 45°$.

Backward reflected TR is observed by the CsI MCP detector at 90° with respect to $\mathbf{v}_b$ by rotating the crystal 90° clockwise from the position shown in Fig. 1. In this geometry no PXR is observed from the surface (100) planes since, as has been previously observed [12,13], PXR is not generated whenever the selection rules [22] for ordinary x-ray diffraction forbid it. These rules exclude the (222) and (100) reflections from face centered cubic crystals such as Si.

Figure 2(b) shows the AD of reflected TR. In this case only 128 frames are required to obtain a useful image. The same color coding described above for Fig. 2(a) is used. In this image $N_{\text{peak}} \sim 240$. We will show below that the TR observed by the CsI MCP is in the vuv region of the spectrum.

Both the PXR and TR AD patterns, which are unfocused in our experiment, are blurred by the finite extent of the beam, since the AD's produced from each segment of the beam overlap when projected onto the plane of the detector. The major effect, a filling in of the center of the AD, is similar to that of true beam divergence, which we have extensively investigated for OTR [19]. The effective divergence $\sigma_{\text{eff}} \cong d_b/2z$, where d_b is the beam diameter and z is the distance between the source and the imager. The measured profile from the OTR beam image is approximately Gaussian with $d_b = 1.6$ mm full width at half maximum (FWHM), so that the rms effective divergence $\sigma_{\text{rms}} = 0.85$ mrad.

Figure 3 shows a vertical scan of the TR pattern given in Fig. 2(b) compared to a theoretical fit which incorporates the convolution of a Gaussian distribution of effective divergence angles [19]. The best fit to the data is obtained with a divergence $\sigma = 0.8$ mrad. The error in determining σ is $< 20\%$. The true beam divergence σ_b is not known, but apparently $\sigma_b \ll \sigma$, since $\sigma \simeq \sigma_{\text{rms}}$. The peak TR intensity occurs at the angle γ^{-1}, where γ is the Lorentz factor of the beam. The fit produces a value for γ which agrees with independent magnetic spectrometer measurements.

The perpendicular polarization shown in the image of the TR AD is due to the combined effects of the reflection coefficient of Si, and the response function of the CsI MCP. Since we did not measure the spectrum of the TR in this experiment, and do not have an absolute calibration of the detector response, we have calculated the TR production and modeled the response of the detector in order to obtain the fit to the TR pattern.

The relative detector response function $f_{\text{DR}}(E_p)$ was modeled [23] simply by forming the product of the photon absorption coefficient [24,25] for CsI and the photon energy E_p. The secondary electron quantum yield ζ_s is proportional to f_{DR} and $\zeta_s \gg \zeta_P$, the primary electron quantum yield [23]. Since the CsI MCP is sensitive only to photons with wavelengths $\lambda < 200$ nm, this establishes the long wavelength cutoff. The effective short wavelength cutoff is determined by the falloff of the TR intensity with λ. The reflectivities of silicon for parallel and perpendicular polarizations reflected at 45°, $R_\parallel$ and $R_\perp$, become very small for $\lambda \lesssim 41$ nm. The corresponding TR intensities are respectively proportional to these reflectivities. Thus the detected bandwidth $\Delta\lambda$ is in the vuv region of the spectrum.

Using f_{DR}, we determined the reflection coefficients [24] averaged over $\Delta\lambda$: $\langle R_\parallel \rangle = 0.19$, $\langle R_\perp \rangle = 0.40$. The ratio $\langle R_\perp \rangle / \langle R_\parallel \rangle \simeq 2.0$ explains the strong vertical polarization observed in Fig. 2(b). The fit to the total TR intensity, particularly in the center of the pattern (see Fig. 3), is consistent

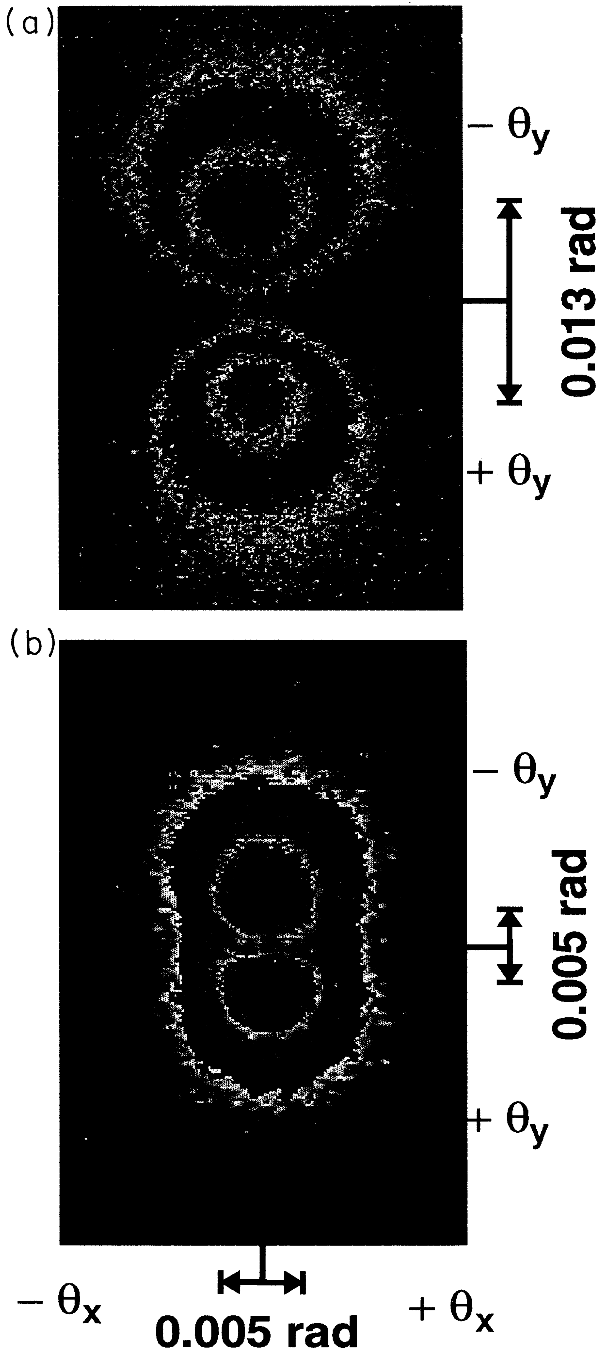

FIG. 2. (a) Vertically polarized angular distribution of PXR from the ⟨022⟩ planes of a 20 μm Si crystal, 45° Bragg angle. (b) Vertically polarized angular distribution of vuv TR from Si, 45° incidence angle [both (a) and (b) have the same angular scales].

with this ratio. If, e.g., $\langle R_\perp \rangle \simeq \langle R_\parallel \rangle$, the pattern would not be polarized, and a much smaller value of σ would have been required to fit the TR data.

As we will show, effects of MS and beam divergence in our experiments have a negligible effect on the measured PXR AD. In this case the angle of peak PXR intensity for a given order is given by $\theta_p = [\gamma^{-2} + |\chi_0(E_p)|]^{1/2}$. At the beam energy of this experiment (230 MeV), and from independent measurement of the susceptibility [26], $|\chi_0| \gg \gamma^{-2}$,

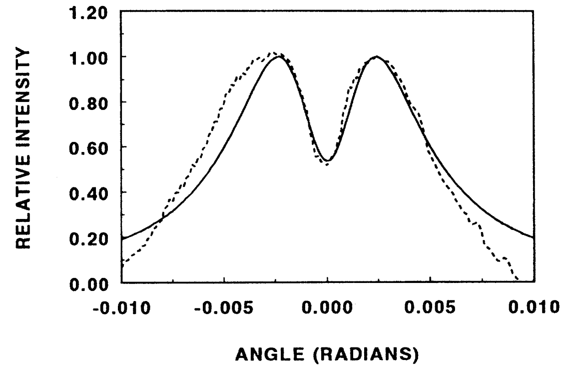

FIG. 3. Vertical scan of intensity as a function of angle θ_y measured from the center of the vuv TR pattern; theory (solid line), data (dotted line).

so that θ_p is determined principally by $|\chi_0|$. This qualitatively explains the larger separation of the peak to peak intensities observed in the PXR pattern compared to the TR, as shown in Figs. 2(a) and 2(b). A similar result from a one dimensional (1D) scan was obtained [7] at $E_b = 900$ MeV.

Theory predicts that the PXR intensity $I \propto L_a$, the absorption length, when the path length of the electrons through the crystal, $L \gg L_a$; and $I \propto L$ when $L_a \gg L$. We have shown in our earlier work [13] on PXR from the ⟨111⟩ planes of Si that a nearly monochromatic (single order) spectrum at 4.56 keV can be generated by choosing $L \sim L_a^{n=1}$. The selection rules forbid the (222) reflection, and higher order intensities are negligible because $L \ll L_a$ for $n > 2$. In the present experiment, where PXR is produced from the ⟨022⟩ planes at $\theta_B = 45°$, the situation is nearly the same, since $E_p^{n=1} = 4.57$ keV, and again $L_a \sim L$. However, the second order (044), which *is* allowed by the selection rules for the ⟨022⟩ planes, contributes about 10% to the total PXR intensity. Higher order contributions are again negligible. In this case, the AD's of the contributing first two orders are superimposed, and the width of the AD for each order will be determined by the corresponding value of $|\chi_0(E_p)|$.

Figure 4 shows a θ_y scan of the PXR pattern compared to theory. The AD's for the individual $n = 1,2$ orders and their sum are shown. For inputs to the theory, we use $|\chi_0(4.57\ \text{keV})| = 4.72 \times 10^{-5}$, and $|\chi_0(9.14\ \text{keV})| = 1.16 \times 10^{-5}$, respectively, which are obtained from the Kramers-Kronig relations and measurements [26] of L_a. As in the vuv TR calculations, we have convolved a Gaussian function of divergence with the single particle PXR distribution, using $\sigma = 0.8$ mrad, which is obtained from the fit to the TR data. The effect of σ on the PXR distribution is indeed negligibly small, as is the effect of MS of the electrons in the crystal ($\theta_{\text{scat}} = 4.8 \times 10^{-4}$ rad $< \sigma$).

The fit to the data is good in the center of the pattern and in the vicinity of the angle of peak emission θ_p but the data fall off faster than theory at angles $|\theta| \gtrsim 1.5\theta_p$. This is most likely due to the response of the detector at low signal levels for which we have only partially compensated using laboratory measurements of the CCD response. We have observed a similar thresholding effect in our early measurements of the AD of OTR, which is very similar to that of the PXR. In these studies the wings and center of the AD were not well observed at very low light levels. This condition increased the errors in measuring the intensities in the wings of the

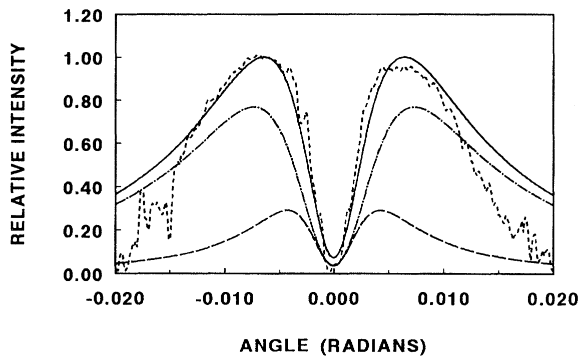

FIG. 4. Vertical scan of intensity as a function of angle θ_y measured from the center of the PXR pattern. Theory: sum of $n=1$ and $n=2$ contributions (solid line); $n=1$ alone (dot-dashed line); $n=2$ alone (dashed line). Data: dotted line.

distribution which, like PXR, fall off more gradually than those in the center of the pattern. The situation was vastly improved when the number of frame integrations was substantially increased. Unfortunately we were limited in these first PXR AD imaging experiments to a maximum integration of 128 frames.

For the above reasons we have concentrated on the comparison of theory to data in the vicinity (50–100%) of the peak PXR emission. By measuring the midpoints of the right and left sidelobes of Fig. 4 at intensities 50–90% of the peak value and extrapolating to 100%, we have determined $\theta_p=6.08$ and 6.61 mrad, for the right and left lobes, respectively. The square of the difference in these values can be used to estimate the error (~16%) that would be made in determining a single value for $|\chi_0|$ from such data. The corresponding theory peaks at 6.4 mrad, which is very close to the average of the measured θ_p's. Other calculations show that the PXR intensity at angles $|\theta|\gtrsim 1.5\theta_p$ is more sensitive to $|\chi_0|$, so that improved data in this region should reduce the error in fitting $|\chi_0|$ for a single order to 5–10%.

In order to achieve such a precision, the signal to noise (S/N) must be improved, and the AD's for each order should be measured. The S/N can be increased by using a cooled imaging detector to reduce background noise, integrating a larger number of images, using higher beam energies, and/or increasing the beam current to increase the PXR photon yield. To isolate the contributions from multiple orders a spectrally sensitive imaging device such as a cooled CCD array used in a counting mode could be employed. With the present detector, which integrates over photon energy, it may also be possible to obtain spectrally resolved images by using filters to progressively eliminate the lower orders.

We have obtained quantitative images of the AD's of PXR and vuv TR. We have obtained values of the beam divergence and estimates of the multiple scattering angle from the vuv TR AD and OTR profile data. Using these, and measured susceptibilities of Si at 4.57 and 9.14 keV, the photon energies produced in the first two orders, we obtain good agreement between the PXR AD data and theory for the observed polarization, angles of peak intensity θ_p, and scans of the AD for angles $|\theta|\lesssim 1.5\theta_p$. Our results indicate that, with improved imaging, it should be possible to use PXR AD's to measure the susceptibility of a single order to an accuracy of 5–10%. Furthermore, by varying the Bragg angle it should be possible to measure $|\chi_0|$ continuously over a wide energy range.

The authors acknowledge the assistance of G. Zoski, J. Barkyoumb (NSWC), A. Pak, S. Thomas, D. Gorzen (XSI), and the SAL technical staff. This work was sponsored in part by DOE SBIR Grant No. DE-FG03-91ER81099; NCI SBIR Grant No. 1-R43-CA60207-01, and the Canadian Natural Science and Engineering Research Council.

[1] V. G. Baryshevsky and I. D. Feranchuk, J. Phys. (Paris) **44**, 913 (1983); Zh. Eksp. Teor. Fiz. **61**, 944 (1971) [Sov. Phys. JETP **34**, 502 (1972)]; **64**, 1190 (1973) [**37**, 605 (1973)]; I. D. Feranchuk and A. V. Ivashin, J. Phys. (Paris) **46**, 1981 (1985).
[2] G. M. Garibyan and C. Yang, Zh. Eksp. Teor. Fiz. **61**, 930 (1971) [Sov. Phys. JETP **34**, 495 (1972)].
[3] V. G. Baryshevsky and I. D. Feranchuk, Nucl. Instrum. Methods Phys. Res. Sect. A **228**, 490 (1985).
[4] R. B. Fiorito *et al.*, Nucl. Instrum. Methods Phys. Res. Sect. B **79**, 758 (1993).
[5] A. N. Didenko, *et al.*, Phys. Lett. A **118**, 363 (1985).
[6] Yu. N. Adishchev *et al.*, Nucl. Instrum. Methods Phys. Res. Sect. B **21**, 49 (1987).
[7] Yu. N. Adishchev *et al.*, Zh. Eksp. Teor. Fiz. **93**, 1943 (1987) [Sov. Phys. JETP **66**, 1107 (1987)].
[8] Yu. N. Adishchev *et al.*, Nucl. Instrum. Methods Phys. Res. Sect. B **44**, 130 (1989).
[9] A. V. Shchagin *et al.*, Phys. Lett. A **148**, 485 (1990).
[10] D. W. Rule *et al.*, Proc. SPIE **1552**, 240 (1991).
[11] K. Yu. Amosov *et al.*, Phys. Rev. E **47**, 2207 (1993).
[12] S. Asano *et al.*, Phys. Rev. Lett. **70**, 3247 (1993).
[13] R. B. Fiorito *et al.*, Phys. Rev. Lett. **71**, 704 (1993).
[14] V. G. Baryshevsky *et al.*, Phys. Lett. **110A**, 477 (1985).
[15] M. L. Ter-Mikelian, *High Energy Electromagnetic Processes in Condensed Media* (Wiley-Interscience, New York, 1972).
[16] M. J. Moran *et al.*, Phys. Rev. Lett. **57**, 1223 (1986).
[17] M. A. Piestrup *et al.*, J. Appl. Phys. **72**, 4300 (1992).
[18] L. Wartski *et al.*, J. Appl. Phys. **46**, 3644 (1975).
[19] R. B. Fiorito and D. W. Rule, in *Beam Instrumentation Workshop, Santa Fe, NM, 1993*, edited by Robert E. Shafer, AIP Conf. Proc. No. 319 (AIP, New York, 1994), pp. 21–37.
[20] G. B. Yodh, in *Coherent Radiation Sources*, edited by A. W. Saenz and H. Uberall (Springer-Verlag, Berlin, 1985).
[21] M. A. Piestrup *et al.*, Appl. Phys. Lett. **59**, 189 (1991).
[22] B. E. Warren, *X-Ray Diffraction* (Addison Wesley, Reading, MA, 1969).
[23] B. L. Henke *et al.*, J. Appl. Phys. **52**, 1509 (1981); M. P. Kowalski *et al.*, Appl. Opt. **25**, 2440 (1986).
[24] *Handbook of Optical Constants of Solids*, edited by Edward D. Palik (Academic, Boston, 1991), Vols. I and II.
[25] M. Cardonna *et al.*, Phys. Rev. B **2**, 1117 (1970); Hiroshi Saito *et al.*, J. Phys. Soc. Jpn. **24**, 1095 (1968).
[26] W. Karstens *et al.*, Bull. Am. Phys. Soc. **36**, 467 (1991); J. Barkyoumb (private communication).

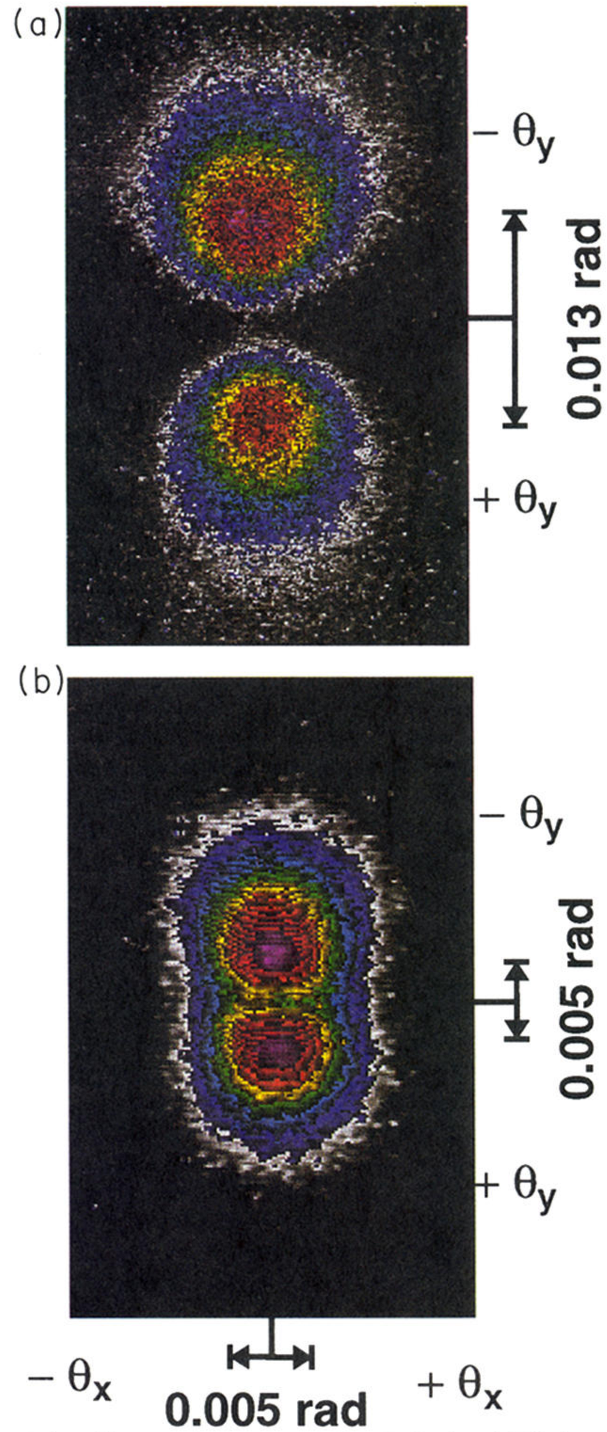

FIG. 2. (a) Vertically polarized angular distribution of PXR from the ⟨022⟩ planes of a 20 μm Si crystal, 45° Bragg angle. (b) Vertically polarized angular distribution of vuv TR from Si, 45° incidence angle [both (a) and (b) have the same angular scales].